Spatiotemporal instabilities in nonlinear bulk media with Bragg gratings

Natalia M. Litchinitser

The Institute of Optics, University of Rochester, Rochester, New York 14627

Colin J. McKinstrie

Department of Mechanical Engineering, University of Rochester, Rochester, New York 14627

C. Martijn de Sterke

School of Physics, University of Sydney, Sydney 2006, Australia

Govind P. Agrawal

The Institute of Optics, University of Rochester, Rochester, New York 14627

Received February 16, 2000; revised manuscript received August 2, 2000

We study spatiotemporal instabilities in a bulk medium with Kerr-type nonlinearity and a volume Bragg grating along the direction of wave propagation. The continuous-wave beam propagation is unstable in such a periodic structure because of an interplay among grating-induced dispersion, diffraction, and nonlinear phase modulation. A linear stability analysis of the nonlinear coupled-mode equations predicts parameters for which novel self-pulsations that occur in both time and space can be observed experimentally. © 2001 Optical Society of America

OCIS codes: 050.2770, 190.3100, 050.1940, 260.0260, 260.2030, 190.0190.

1. INTRODUCTION

Modulational instability (MI) has been extensively investigated in several branches of physics.[1–7] It refers to a phenomenon that reveals itself as the exponential growth of weak perturbations when an intense pump beam propagates inside a nonlinear medium. For example, in plasma physics, MI of high-intensity laser beams results in the formation of hot spots in the transverse intensity profile of the beam.[3,4] In the case of optical fibers, MI manifests itself as breakup of the continuous-wave (cw) or quasi-cw radiation into a train of short optical pulses.[2]

Generally, MI's can be classified as temporal (longitudinal) or spatial (transverse), depending on whether a cw beam disperses or diffracts inside the nonlinear medium. These instabilities can occur when a single intense beam propagates through the medium as well as when several laser beams propagate at once. Temporal MI of a single wave in optical fibers has been observed in the anomalous-dispersion regime.[5] It was shown that temporal and spatial instabilities can, in fact, occur simultaneously in a bulk nonlinear medium when diffraction and dispersion take place simultaneously.[8] In this case, MI can occur in both anomalous- and normal-dispersion regimes. In parallel to these investigations, several authors have considered the propagation of two waves in nonlinear media. It has been shown that even when single-wave propagation is stable, MI can develop in the presence of another, copropagating or counterpropagating, wave.[3,9] These studies addressed the spatial MI of two collinear waves in a three-dimensional dispersionless nonlinear medium[3] as well as the temporal MI of two waves in a one-dimensional dispersive nonlinear medium.[9,10] More recently, MI for counterpropagating waves was observed experimentally in Bragg gratings.[11–14] In this case forward- and backward-propagating waves are coupled both linearly (as a result of periodicity) and nonlinearly (as a result of the Kerr effect).[15] It is well known that a periodic structure introduces strong dispersion at frequencies close to the edges of the photonic bandgap.[16,17] Theoretical investigation of MI in one-dimensional periodic structures[6] revealed several new features of MI in the anomalous-dispersion regime at high powers. In particular, it was found that even in the normal-dispersion regime the cw field may become unstable.

Most of the research on MI in periodic structures has been confined to temporal instabilities. Spatial instabilities were considered in Refs. 18 and 19. However, in those investigations either instabilities in a finite periodic structure under bidirectional illumination[19] or stability of nonlinear Bloch waves in a semi-infinite periodic medium[18] were considered. Our aim in this study is to present a detailed investigation of spatiotemporal instabilities of two counterpropagating waves in an infinite geometry, as shown in Fig. 1. This paper is organized as follows: In Section 2, after reviewing coupled-mode theory describing the propagation of light in nonlinear periodic structures, we develop the linear stability analysis

0740-3224/2001/010045-10$15.00

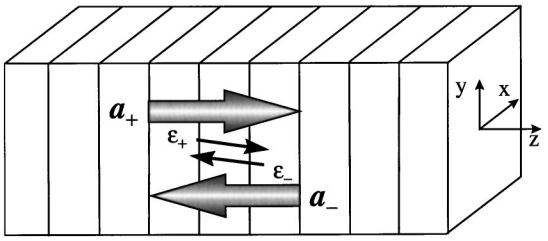

Fig. 1. Schematic illustration of a bulk nonlinear periodic structure.

to study spatiotemporal instabilities in such structures. In Sections 3–6 we analyze various regimes of the spatiotemporal MI's, and in Section 7 we identify their physical origins. In Section 8 we discuss the experimental conditions and materials that one can use to observe spatiotemporal MI in periodic structures. Finally, we present a summary of our results in Section 9.

2. THEORY

A. Propagation Equations

Wave propagation in Bragg gratings can be described by use of the nonlinear coupled-mode equations. These equations are valid only for shallow gratings and for wavelengths close to the Bragg wavelength. The nonlinear coupled-mode equations can be derived by substitution of the following form for electric field E:

$$E = [E_+ \exp(+ik_B z) + E_- \exp(-ik_B z)]\exp(-i\omega_B t) \quad (1)$$

into the wave equation. Here E_+ and E_- are the slowly varying amplitudes of forward- and backward-propagating waves, respectively, and $k_B = \pi/\Lambda$ is the wave number at the Bragg frequency $\omega_B = \pi c/(n\Lambda)$. The resultant nonlinear coupled-mode equations for $E_\pm$ can be written as

$$i\frac{\partial E_+}{\partial z} + i\frac{1}{V}\frac{\partial E_+}{\partial t} + \frac{1}{2k_B}\left(\frac{\partial^2 E_+}{\partial x^2} + \frac{\partial^2 E_+}{\partial y^2}\right) + \kappa E_- + \Gamma(|E_+|^2 + 2|E_-|^2)E_+ = 0, \quad (2)$$

$$-i\frac{\partial E_-}{\partial z} + i\frac{1}{V}\frac{\partial E_-}{\partial t} + \frac{1}{2k_B}\left(\frac{\partial^2 E_-}{\partial x^2} + \frac{\partial^2 E_-}{\partial y^2}\right) + \kappa E_+ + \Gamma(|E_-|^2 + 2|E_+|^2)E_- = 0, \quad (3)$$

where $V = c/n$ is the velocity of light in the absence of a grating, $\kappa = \pi\Delta n/\lambda_B$ is the coupling coefficient, Δn is the index-modulation depth, and $\lambda_B = 2n\Lambda$ is the Bragg wavelength. The nonlinear parameter Γ is defined as $\Gamma = 2\pi n_2/\lambda_B$, where n_2 is the nonlinear refractive index. In this study we use chalcogenide glass as an example of a nonlinear medium. The nonlinear refractive index of chalcogenide glass is ~100 times larger than that in silica glasses.[20,21] Also, it has been shown that chalcogenide glass when it is exposed to visible light exhibits a change in linear refractive index that can be as high as 0.01.[20] Indeed, As_2S_3-based fiber Bragg gratings were recently reported.[20] Various types of chalcogenide glass have been investigated, and high-quality, single-mode chalcogenide-glass waveguides operating near 1.55-μm have been demonstrated.[21]

In the case of counterpropagating cw plane waves of constant intensity, Eqs. (2) and (3) can be solved analytically, as we assume that $E_\pm$ are then independent of x and y. The solution can be written as[6]

$$E_+ = \frac{a}{\sqrt{f^2+1}}\exp[i(Qz - \Omega Vt)] \equiv a_+ \exp[i(Qz - \Omega Vt)], \quad (4)$$

$$E_- = \frac{af}{\sqrt{f^2+1}}\exp[i(Qz - \Omega Vt)] \equiv a_- \exp[i(Qz - \Omega Vt)], \quad (5)$$

where a and f are two real parameters and

$$\Omega = -\frac{\kappa}{2}(f^{-1} + f) - \frac{3}{2}\Gamma a^2, \quad (6)$$

$$Q = -\frac{\kappa}{2}(f^{-1} - f) - \frac{1}{2}\Gamma a^2\frac{1-f^2}{1+f^2}. \quad (7)$$

Parameter a is related to the total power in the grating through $a^2 = |E_+|^2 + |E_-|^2$, whereas parameter f determines the position on the dispersion curve in the Ω–Q plane and is related to the group velocity: $v_g = V(d\Omega/dQ) = V(1-f^2)/(1+f^2)$. Physically, parameter f represents the ratio of forward- and backward-propagating waves; i.e., $f = E_-/E_+$.

Let us first describe the dispersive characteristics of the periodic structure in the low-power limit $a \ll 1$ by setting $\Gamma = 0$. Figure 2 shows the dispersion relation $\Omega(Q)$ in the limit $a \to 0$ for both a uniform medium (dashed lines) and a periodic medium (solid curves). For Ω in the range $-\kappa \leq \Omega \leq \kappa$, that defines the photonic bandgap, no propagating wave solutions are allowed and most of the light is reflected. Outside this region, light can propagate inside the periodic structure. In the absence of the grating, light propagates at the speed of light in the

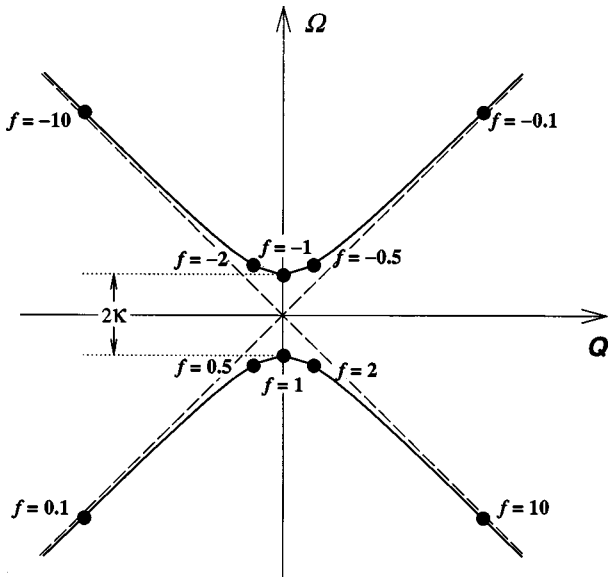

Fig. 2. Dispersion curves for an infinite linear periodic structure.

uniform medium. The grating introduces a curvature in the dispersion curve, as shown in Fig. 2, that leads to dispersion at frequencies close to the edges of the photonic bandgap. On the upper branch of the dispersion curve, corresponding to $f < 0$, the group-velocity dispersion of the grating is negative (anomalous GVD). On the lower branch, corresponding to $f > 0$, the qroup-velocity dispersion is positive (normal GVD). At frequencies close to the edge of the photonic bandgap, the grating also exhibits significant higher-order dispersion.[16,17,22] The special cases $f = \pm 1$ correspond to the two edges of the photonic bandgap; in particular, $f = -1$ coincides with the top of the bandgap and $f = 1$ with the bottom of the bandgap. In the low-power limit, the top and the bottom of the photonic bandgap correspond to $\Omega = \kappa$ and $\Omega = -\kappa$, respectively, where $\Omega = V^{-1}(\omega_0 - \omega_B)$, ω_0 is the frequency of the light [s^{-1}], and ω_B is the Bragg frequency [s^{-1}]. Also, $|f| < 1$ corresponds to forward propagation and $|f| > 1$ to backward propagation.

B. Linear Stability Analysis

In this section we return to the nonlinear case. In general, Eqs. (2) and (3) should be solved numerically. However, the stability of the cw solution can be studied analytically with standard linear stability analysis. The basic idea of this analysis consists of perturbing the cw solution slightly and studying whether this small perturbation grows or decays with propagation. Of course, such an analysis can provide only the initial growth of perturbation. When the perturbation amplitude grows enough to become comparable with that of the incident beam, a numerical analysis becomes necessary.

Using a standard procedure, we assume that solutions (4) and (5) are perturbed slightly such that

$$E_{\pm} = [a_{\pm} + \varepsilon_{\pm}(x, y, z, t)]\exp[i(Qz - \Omega Vt)], \quad (8)$$

with the perturbation $|\varepsilon_{\pm}| \ll a_{\pm}$. Substituting Eq. (8) into Eqs. (2) and (3) and linearizing in $\varepsilon_{\pm}$, we obtain the following two linear equations:

$$i\frac{\partial \varepsilon_+}{\partial z} + i\frac{1}{V}\frac{\partial \varepsilon_+}{\partial t} + \frac{1}{2k_B}\left(\frac{\partial^2 \varepsilon_+}{\partial x^2} + \frac{\partial^2 \varepsilon_+}{\partial y^2}\right) + \kappa\varepsilon_- - f\kappa\varepsilon_+ + G[(\varepsilon_+ + \varepsilon_+^*) + 2f(\varepsilon_- + \varepsilon_-^*)] = 0, \quad (9)$$

$$-i\frac{\partial \varepsilon_-}{\partial z} + i\frac{1}{V}\frac{\partial \varepsilon_-}{\partial t} + \frac{1}{2k_B}\left(\frac{\partial^2 \varepsilon_-}{\partial x^2} + \frac{\partial^2 \varepsilon_-}{\partial y^2}\right) + \kappa\varepsilon_+ - f^{-1}\kappa\varepsilon_- + G[2f(\varepsilon_+ + \varepsilon_+^*) + f^2(\varepsilon_- + \varepsilon_-^*)] = 0, \quad (10)$$

where $G = \Gamma a^2/(1 + f^2)$. Also, for the following discussion it is convenient to define a parameter $P = \Gamma a^2$ that is proportional to the total beam power and is inversely related to the nonlinear length [$L_{\mathrm{NL}} = 1/\Gamma(a^2)$].[2]

We assume plane-wave solutions for $\varepsilon_{\pm}$ of the form

$$\varepsilon_{\pm}(x, y, z, t) = b_{\pm}\exp[i(\mathbf{K} \cdot \mathbf{r} - \omega Vt)] + c_{\pm}\exp[-i(\mathbf{K} \cdot \mathbf{r} - \omega Vt)], \quad (11)$$

where b_+ and c_+ correspond to forward sidebands and b_- and c_- correspond to backward sidebands.

Substituting Eq. (11) into Eqs. (9) and (10), we obtain four linear coupled equations for $b_{\pm}$ and $c_{\pm}$:

$$(\omega - k_{\|} - \kappa f + G - k_t^2)b_+ + Gc_+ + (\kappa + 2fG)b_- + 2fGc_- = 0, \quad (12a)$$

$$Gb_+ + (-\omega + k_{\|} - \kappa f + G - k_t^2)c_+ + 2fGb_- + (\kappa + 2fG)c_- = 0, \quad (12b)$$

$$(\kappa + 2fG)b_+ + 2fGc_+ + (\omega + k_{\|} - \kappa f^{-1} + f^2G - k_t^2)b_- + f^2Gc_- = 0, \quad (12c)$$

$$2fGb_+ + (\kappa + 2fG)c_+ + f^2Gb_- + (-\omega - k_{\|} - \kappa f^{-1} + f^2G - k_t^2)c_- = 0, \quad (12d)$$

where $k_t = K_t/\sqrt{2k_B}$, $K_t = \pm\sqrt{K_x^2 + K_y^2}$ is the transverse component, and $k_{\|} = K_z$ is the longitudinal component of $\mathbf{K}$. Equations (12) have a nontrivial solution only if the determinant of the coefficient matrix vanishes. The determinant establishes the dispersion relation $\omega(\mathbf{K})$ that the perturbation must satisfy.

We present our results in the next four sections: In Sections 3 and 4 we consider two special cases ($f = \pm 1$) for which the cw beam is exactly tuned to the top and the bottom of the photonic bandgap. In Sections 5 and 6 we discuss the effects of detuning from the bandgap edges. The dispersion relation obtained from Eqs. (12) is a quartic polynomial in ω whose roots require, in general, numerical evaluation for arbitrary values of f.

3. TOP OF THE PHOTONIC BANDGAP

The case $f = -1$ corresponds to tuning the cw beam to the top of the photonic bandgap. Inasmuch as the dispersion is anomalous on the upper branch of the dispersion relation, we expect temporal MI because of the mutual effect of the dispersion and Kerr nonlinearity in this regime. At the same time we also expect spatial MI that results from an interplay between transverse effects and the nonlinearity.

In this case the determinant of the coefficient matrix of Eqs. (12) is simplified significantly and the roots can therefore be found analytically. Solving Eqs. (12) when $f = -1$, we find that

$$\omega^2 = 2\kappa^2 - 2G\kappa + k_{\|}^2 - 2\kappa k_t^2 - 2Gk_t^2 + k_t^4 \pm 2(\kappa^4 - 2G\kappa^3 + G^2\kappa^2 + k_{\|}^2\kappa^2 + 2Gk_{\|}^2\kappa - 2k_t^2\kappa^3 + 6Gk_t^2\kappa^2 - 4G^2k_t^2\kappa - 2\kappa k_{\|}^2k_t^2 - 2Gk_{\|}^2k_t^2 + \kappa^2k_t^4 - 4G\kappa k_t^4 + 4G^2k_t^4 + k_{\|}^2k_t^4)^{1/2}. \quad (13)$$

The instability is associated with the imaginary part of $\omega = \omega_r + i\omega_i$ because the perturbation then grows exponentially with time, as one can see from Eq. (11). We can find the boundaries of the unstable region in the parameter space ($k_{\|}$, k_t) by finding values of $k_{\|}$ for which $\omega^2 = 0$.

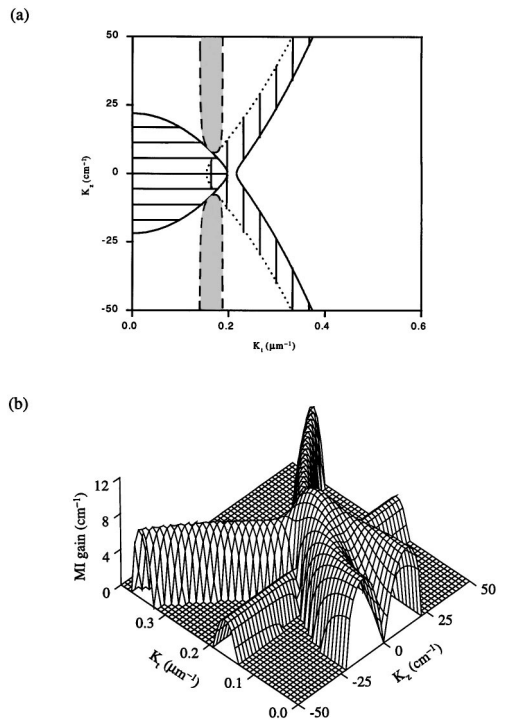

Fig. 3. (a) Instability domains in **K** space and (b) the corresponding gain for the top of the photonic bandgap ($\kappa = 10\ \mathrm{cm}^{-1}$, $P = 8\ \mathrm{cm}^{-1}$).

It can be shown that the right-hand side of Eq. (13) vanishes when

$$k_{\parallel}^{(1)} = \pm(12G\kappa - 6Gk_t^2 - 2\kappa k_t^2 + k_t^4)^{1/2} \quad (14)$$

or when

$$k_{\parallel}^{(2)} = \pm(2Gk_t^2 - 2\kappa k_t^2 + k_t^4)^{1/2}. \quad (15)$$

Note also that, when

$$k_{\parallel}^{(3)} = \pm\left(\frac{\kappa^4 - 2G\kappa^3 + G^2\kappa^2 - 2k_t^2\kappa^3 + 6G\kappa^2k_t^2 - 4G^2\kappa k_t^2 + \kappa^2k_t^4 - 4G\kappa k_t^4 + 4G^2k_t^4}{-\kappa^2 - 2G\kappa + 2\kappa k_t^2 + 2Gk_t^2 - k_t^4}\right)^{1/2}, \quad (16)$$

the argument of the square root in Eq. (13) vanishes. When the argument becomes negative, ω is complex, and therefore instabilities also occur for these values of $k_{\parallel}$.

Instability regions given by Eqs. (14)–(16) are shown in Fig. 3(a), where the solid curves correspond to $k_{\parallel}^{(1)}$, the long-dashed curves to $k_{\parallel}^{(2)}$, and the short-dashed curve to $k_{\parallel}^{(3)}$. Figure 3(b) shows MI gain $\gamma = \mathrm{Im}(\omega)$ as a function of K_z and K_t. In the one-dimensional case [in the absence of transverse terms in Eqs. (2) and (3)], MI gain reduces to that found in Ref. 6 for a fiber Bragg grating if we set $K_t = 0$. However, in the presence of transverse effects induced by diffraction, the instability that is due to spatial modulation accompanies temporal instability. As can be seen from Fig. 3(b), the maximum gain occurs at a nonzero value of K_t; in fact, maximum gain corresponds to $K_z = 0$. This means that the MI is a pure spatial effect and would lead to a ring pattern on the transverse intensity profile of the cw beam because of cylindrical symmetry. However, if the perturbation is seeded at other values of K_z and K_t, both temporal and spatial instabilities can develop simultaneously. This situation can be visualized as a transverse ring pattern oscillating in time.

One may ask whether the gain peak always occurs at $K_t \neq 0$ when diffractive effects are included. We can answer this question qualitatively by expanding the gain $\gamma(K_z, K_t)$ in the neighborhood of $(K_z^{\max}, 0)$, where $K_z^{\max}$ is the location of the gain peak in the one-dimensional case,[6] and study whether this point remains a local gain maximum in the three-dimensional case. We find that the gain peak always shifts to $K_t \neq 0$ when $\kappa > G$. In fact, point $(K_z^{\max}, 0)$ is a saddle point in this case. In the limit $G > \kappa$, the local maximum still occurs at point $(K_z^{\max}, 0)$ although the global maximum is found to occur numerically at $K_t \neq 0$. Although such was not proved rigorously, we find that a global maximum (when $f = -1$) always occurs at $K_z = 0$. Substituting $K_z = 0$ into Eq. (13), we find that the gain peak occurs at $K_t^{\max} = \sqrt{6Gk_B}$ and is equal to $\gamma = 3G$. Comparing this value with the value of gain at point $(K_z^{\max}, 0)$ which is equal to $\gamma = 3G\,[\kappa/(\kappa + 2G)]^{1/2}$, we conclude that the gain is always higher at $K_t \neq 0$.

Another noteworthy feature, shown in Fig. 3(b), is that the instabilities can occur for arbitrarily large values of K_t. In the single-wave case, in both one-dimensional[2] and three-dimensional[8] geometries the instability region for anomalous dispersion is always bounded. However, the MI region is always unbounded for two counterpropagating waves in dispersionless three-dimensional media[23] and, in fact, looks similar to what we observe for large K_z and K_t in Fig. 3. These qualitative observations suggest that we should consider two limiting cases: (1) a bulk nonlinear medium without a grating ($\kappa \to 0$) and (2) a one-dimensional periodic structure (no transverse effects). Let us consider each of them in more detail.

A. Bulk Kerr Medium Without a Grating

For a bulk Kerr medium without a grating, Eqs. (2) and (3) reduce to those studied in Ref. 23 in the context of

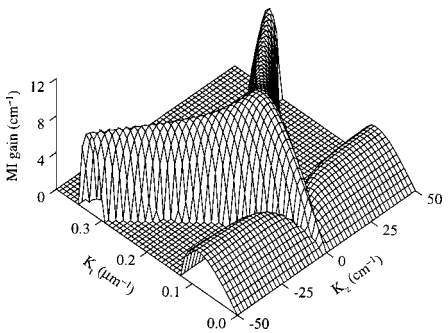

Fig. 4. Instability gain under conditions identical to those of Fig. 3, except that $\kappa = 0$ (no grating, no dispersion).

plasma physics and describe the dispersionless evolution of two counterpropagating waves coupled only through the nonlinearity. Therefore the results of the analysis of Ref. 23 can be directly applied here. We find the following relation among ω, $k_\parallel$, and k_t:

$$\omega^2 = k_\parallel^2 - 2Gk_t^2 + k_t^4 \pm 2(4G^2k_t^2 - 2G^2k_\parallel^2k_t^2 + k_\parallel^2k_t^4)^{1/2}. \quad (17)$$

Figure 4 shows the MI gain given by Eq. (17). Figures deed, the instability regions are unbounded in both cases,

Following the analysis in Section 3, we find the boundaries of the regions in parameter space $(k_\parallel, k_t)$ where instabilities occur. The right-hand side of Eq. (19) vanishes when

$$k_\parallel^{(5)} = \pm(-12G\kappa - 6Gk_t^2 + 2\kappa k_t^2 + k_t^4)^{1/2} \quad (20)$$

or when

$$k_\parallel^{(6)} = \pm(2Gk_t^2 + 2\kappa k_t^2 + k_t^4). \quad (21)$$

Also, the argument of the square root in Eq. (19) vanishes when

$$k_\parallel^{(7)} = \pm\left(\frac{\kappa_4 + 2G\kappa^3 + G^2\kappa^2 + 2k_t^2\kappa^3 + 6G\kappa^2k_t^2 + 4G^2\kappa k_t^2 + \kappa^2k_t^4 + 4G\kappa k_t^4 + 4G^2k_t^4}{-\kappa^2 + 2G\kappa - 2\kappa k_t^2 + 2Gk_t^2 - k_t^4}\right)^{1/2}. \quad (22)$$

and the absolute maximum occurs at $K_z = 0$. Therefore, at large K_z and K_t, a grating seems irrelevant. At small K_z and K_t, grating-induced dispersion in combination with Kerr nonlinearity (and transverse effects) modifies MI gain such that a doughnutlike gain shape appears in Fig. 3(b). This behavior is similar to that of the single wave propagating in the volume dispersive nonlinear medium studied in Ref. 8.

B. One-Dimensional Periodic Structure

When $K_t = 0$, Eq. (13) becomes identical to the dispersion relation found in Ref. 6. Therefore, in this case our results reduce to those obtained for a one-dimensional periodic structure such as a fiber Bragg grating. Indeed, from Eqs. (14)–(16), the borders of instability are given by

$$k_\parallel^{(4)} = \pm\sqrt{12G\kappa}, \quad (18)$$

an equation that is identical to that obtained in Ref. 6. We thus find that the wave numbers that correspond to the largest gain are identical to those in Ref. 6. As we showed above, those wave numbers do not correspond to a global maximum of the gain in a full three-dimensional problem (see Fig. 3).

4. BOTTOM OF THE PHOTONIC BANDGAP

Let us now consider the case when $f = 1$, which corresponds to tuning the cw beam to the bottom of the photonic bandgap. In Ref. 6 it was shown that, despite the normal dispersion on the lower branch of the dispersion curve, temporal MI can occur. In our case, we also expect spatial MI to occur, as a result of the mutual effect of transverse effects and nonlinearity.

The determinant in Eq. (12) can be simplified in this case, and we obtain the following analytic expression for the dispersion relation:

$$\omega^2 = 2\kappa^2 + 2G\kappa + k_\parallel^2 + 2k_t^2\kappa - 2Gk_t^2 + k_t^4 \pm 2(\kappa^4 + 2G\kappa^3 + G^2\kappa^2 + k_\parallel^2\kappa^2 - 2G\kappa k_\parallel^2 + 2\kappa^3k_t^2 + 6G\kappa^2k_t^2 + 4G^2\kappa k_t^2 + 2\kappa k_\parallel^2k_t^2 - 2Gk_\parallel^2k_t^2 + \kappa^2k_t^4 + 4G\kappa k_t^4 + 4G^2k_t^4 + k_\parallel^2k_t^4)^{1/2}. \quad (19)$$

Again, when the argument becomes negative, ω is complex, and therefore instabilities occur also for these values of $k_\parallel$.

We plot the instability regions given by Eqs. (20)–(22) in Fig. 5(a) and the MI gain in Fig. 5(b). Note that in this example we have used a higher input power P than in the previous case because, as was shown in Ref. 6, there is a finite threshold for grating-induced instabilities in normal dispersion. Consider again the two limiting cases. When $\kappa \to 0$, Eqs. (2) and (3) become dispersionless, and therefore we would expect the MI gain to be identical for both signs of parameter f. To investigate how the grating modifies the gain, we compare Fig. 5(b) with Fig. 4 and find that at large K_z and K_t the figures are quite similar (note that the input powers used in these figures are different, so the comparison is only qualitative). Therefore the grating affects the gain only for small wave numbers.

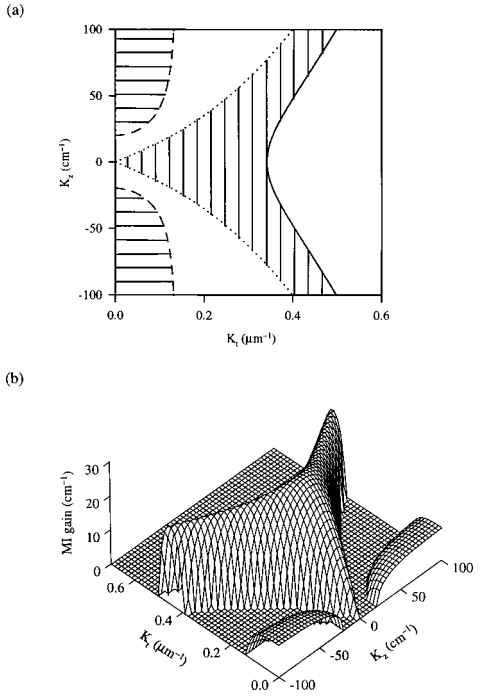

Fig. 5. (a) Instability domains and (b) the corresponding gain for the bottom of the photonic bandgap ($\kappa = 10\,\mathrm{cm}^{-1}$, $P = 20\,\mathrm{cm}^{-1}$).

This result is not unexpected, as grating effects are not significant away from the Bragg resonance. In particular, the grating provides the gain at $K_t = 0$, which is zero without the grating. This case was discussed in detail in Ref. 6. Here we only stress that our results reduce to those in Ref. 6 in the appropriate limit.

5. ANOMALOUS-DISPERSION REGIME ($f < 0$)

So far we have studied the instabilities only at the two edges of the photonic bandgap. This is where forward- and backward-propagating waves are strongly coupled because of the presence of the grating. In the general case of arbitrary f, Eqs. (12) can be written as

$$\begin{aligned}(\omega - \omega_1)(\omega - \omega_2)(\omega - \omega_3)(\omega - \omega_4) \\ - 12fG^2k_t^2(\kappa + \kappa f^2 + fk_t^2) - G[-12\kappa f k_\parallel^2 \\ - 2k_\parallel^2 k_t^2 - 2f^2k_\parallel^2 k_t^2 + 4(f^2 - 1)k_\parallel k_t^2\omega] \\ - 2Gf^{-2}[\kappa^2 k_t^2 + 5\kappa^2 f^2 k_t^2 + 5\kappa^2 f^4 k_t^2 + \kappa^2 f^6 k_t^2 \\ + 2\kappa f k_t^4 + 6\kappa f^3 k_t^4 + 2\kappa f^5 k_t^4 + f^2 k_t^6 + f^4 k_t^6 \\ + 2\kappa f^3\omega^2 - f^2 k_t^2\omega^2 - f^4 k_t^2\omega^2] = 0, \quad (23)\end{aligned}$$

where the linear roots $(\omega_1, \omega_2, \omega_3, \omega_4)$ are given by

$$\omega_{1,2} = \frac{\kappa}{2}(f^{-1} + f) \pm [k_\parallel^2 - k_\parallel(f^{-1} - f) + {}^1\!/_4(f^{-1} + f)^2]^{1/2} + k_t^2, \quad (24)$$

$$\omega_{3,4} = -\frac{\kappa}{2}(f^{-1} + f) \pm [k_\parallel^2 + k_\parallel(f^{-1} - f) + {}^1\!/_4(f^{-1} + f)^2]^{1/2} - k_t^2. \quad (25)$$

Equations (24) and (25) are almost identical to the linear roots found in Ref. 6, the only difference, is that the last term, because of the transverse effects, introduces a shift of these roots.

Let us consider the case when the initial cw wave is detuned from the edge of the photonic bandgap into the anomalous-dispersion regime ($f < 0$). We have studied a large number of cases for various incident intensities and detunings from the edge of the photonic bandgap. Some representative examples are shown in Fig. 6. At low intensities the gain curve resembles that for the single-wave case, as discussed by Liou *et al.*[8]; i.e., it has a doughnutlike shape with equal maximum gain for frequencies equidistant from the center [Fig. 6(a)]. At higher intensities an absolute maximum occurs at $K_z = 0$ (*but* $K_t \neq 0$), which means that the spatial effects dominate temporal ones, as shown in Fig. 6(b). Figures 6(c) and 6(d) show that, if the frequency of the incident beam lies far from the edge of the photonic bandgap, nearly the same gain occurs for a range of frequencies; i.e., there is no well-isolated absolute peak at the gain surface. This result implies that if the instability develops from the noise several different frequencies will have equal chances to grow. In general in this regime both spatial and temporal instabilities exist for any incident intensity.

6. NORMAL-DISPERSION REGIME ($f > 0$)

In this section we consider the case when the frequency of the initial cw wave lies upon the lower branch of the dispersion relation where dispersion is normal. Several representative examples of the gain curves are shown in Fig. 7.

In Ref. 6 it was shown that there is a finite threshold below which the cw wave is stable. This threshold is given by $Gf > \kappa/(2f^2)$ for $f > 1$ and by $Gf > \kappa f^2/2$ for

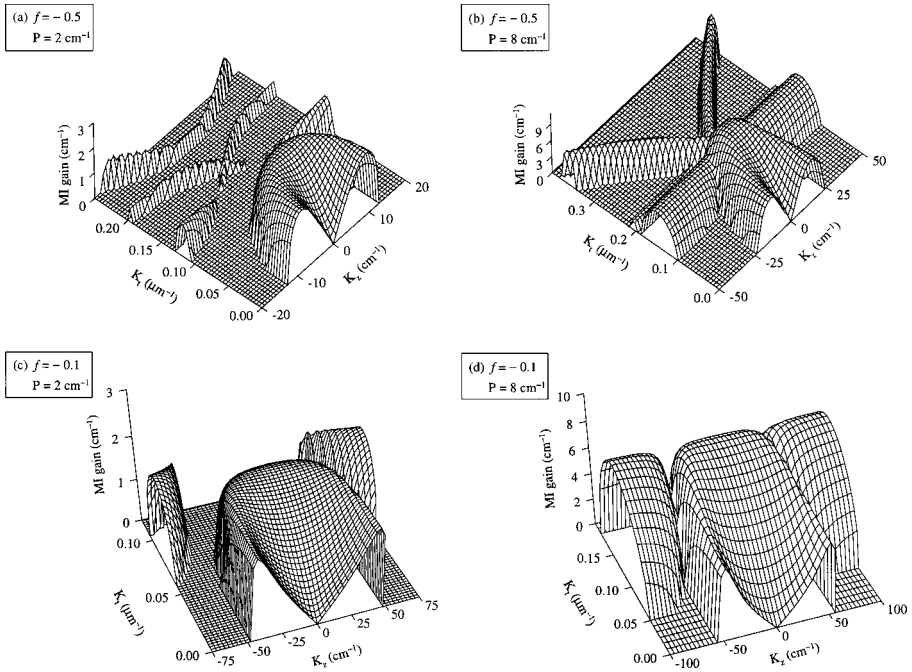

Fig. 6. MI gain in the **K** space for values of f and P as shown. In all cases $\kappa = 10\,\mathrm{cm}^{-1}$.

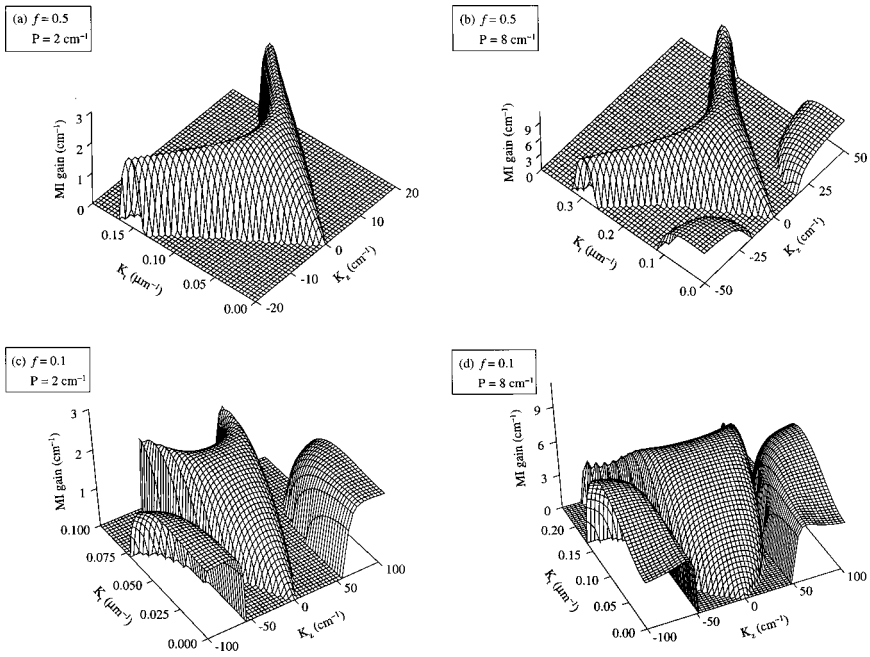

Fig. 7. MI gain in **K** space for values of f and P as shown.

$f < 1$. The parameters used in Fig. 7(a) correspond to the below-threshold case. However, instability still occurs because of the spatial effects. However, for incident intensities that exceed the threshold [Figs. 7(b)–7(d)] both spatial and temporal instabilities can develop. If we compare Figs. 7(b)–7(d) with Fig. 4 we notice again that grating modifies the gain curves primarily for small transverse wave numbers, that is, it permits growth that does not exist in the absence of the grating.

7. PHYSICAL INTERPRETATION

To understand the origin of various features of the gain curves shown in Figs. 3–7 it is advantageous to consider in detail the interaction among the four sidebands that are hidden in the dispersion equation. Let us consider various kinds of two-sideband process. These include forward four-wave mixing (FFWM), which involves either forward pump wave a_+ and its two sidebands b_+ and c_+ or backward pump wave a_- and its corresponding sidebands b_- and c_-. One should also consider backward four-wave mixing processes (BFWM) that involve interactions between one forward and one backward sideband (b_+, c_-) or (c_+, b_-). The third possibility is the interaction between pair of sidebands (b_+, b_-) and pair of sidebands (c_+, c_-); however, we have not found any instabilities that result from this process.

A. Forward Four-Wave Mixing

First let us consider the interaction of the sidebands associated with the forward pump wave, namely, b_+ and c_+, and ignore all other interactions. Then from Eqs. (12) we obtain

$$\begin{bmatrix} \omega - k_\parallel - \kappa f + G - k_t^2 & G \\ G & -\omega + k_\parallel - \kappa f + G - k_t^2 \end{bmatrix} = 0, \quad (26)$$

which gives

$$\omega = k_\parallel \pm \sqrt{\kappa f + k_t^2}\sqrt{\kappa f - 2G + k_t^2}. \quad (27)$$

Let us first analyze the case of $f < 0$. Instabilities occur only when

$$-\kappa|f| + k_t^2 > 0, \quad -\kappa|f| - 2G + k_t^2 < 0. \quad (28)$$

Then the instability gain is given by

$$\gamma = \sqrt{-\kappa|f| + k_t^2}\sqrt{\kappa|f| + 2G - k_t^2}. \quad (29)$$

Maximizing the right-hand side of the Eq. (29), we find the wave number that corresponds to the largest gain:

$$k_t = \pm\sqrt{G + \kappa|f|}. \quad (30)$$

The maximum gain is then given by

$$\gamma^{\max} = G. \quad (31)$$

Figure 8(a) shows the FFWM-induced gain for $f = -1$. Comparing Figs. 8(a) and 3(b), we can easily identify FFWM-induced branches in Fig. 3(b). Inasmuch as one of the main goals of this study is understanding the effect of the grating on the MI gain, in Fig. 8(b) we plot the FFWM gain for case $\kappa = 0$. Then, comparing Figs. 8(a) and 8(b), we conclude that in the anomalous-dispersion regime the grating shifts the FFWM-induced branches of the gain along K_t. Note that here we consider a forward-propagating pump and its sidebands. A similar analysis can be made for a backward-propagating pump, the only difference coming from the ratio between the forward- and backward-propagating wave amplitudes given by parameter f.

Now we consider the case $f > 0$. Instabilities occur only when $\kappa f - 2G + k_t^2 < 0$. The instability gain is then given by

$$\gamma = \sqrt{\kappa f + k_t^2}\sqrt{2G - \kappa f - k_t^2}. \quad (32)$$

We can find the wave number that corresponds to the largest gain by maximizing the right-hand side of Eq. (32), which leads to

$$k_t = 0 \qquad \kappa f > G > \kappa f/2,$$

or

$$k_t = \pm\sqrt{G - \kappa f} \qquad G > \kappa f, \tag{33}$$

and the maximum gain is then given by

$$\gamma^{\max} = \sqrt{\kappa f}\sqrt{2G - \kappa f},$$

$$\gamma^{\max} = G, \tag{34}$$

respectively.

In Fig. 8(c) we plot the FFWM-induced gain for $f = 1$ for the parameters used in Fig. 5(b). As in the previous case, in Fig. 8(d) we plot the FFWM-induced gain for $\kappa = 0$ [note that it should be similar to that for Fig. 8(b), except that different input powers have been used (see the figure captions)]. Comparing Figs. 8(c) and 8(d), we conclude that the grating significantly modifies the FFWM-induced instability gain near $K_t = 0$; in particular, it provides a nonzero gain at $K_t = 0$.

B. Backward Four-Wave Mixing

In this subsection we study the interaction of two sidebands propagating in opposite directions. The process is known as BFWM. First let us consider the interaction of the sideband associated with forward pump wave, b_+, and the sideband associated with backward pump wave, c_-. In this case the dispersion relation [Eqs. (12)] reduces to

$$\begin{bmatrix} \omega - k_\parallel - \kappa f + G - k_t^2 & 2fG \\ 2fG & -\omega - k_\parallel - \kappa f^{-1} + f^2 G - k_t^2 \end{bmatrix} = 0, \tag{35}$$

which leads to

$$\omega = 0.5 f^{-1}\{-fG + f^3 G - \kappa + \kappa f^2 \pm [(fG - f^3 G + \kappa - \kappa f^2)^2 - 4f(3f^3 G^2 + G\kappa + \kappa G f^4 - f\kappa^2 + fGk_\parallel + f^3 Gk_\parallel - \kappa k_\parallel - \kappa f^2 k_\parallel - fk_\parallel^2 + fGk_t^2 + f^3 Gk_t^2 - \kappa k_t^2 - \kappa f^2 k_t^2 - 2fk_\parallel k_t^2 - fk_t^4)]^{1/2}\}. \tag{36}$$

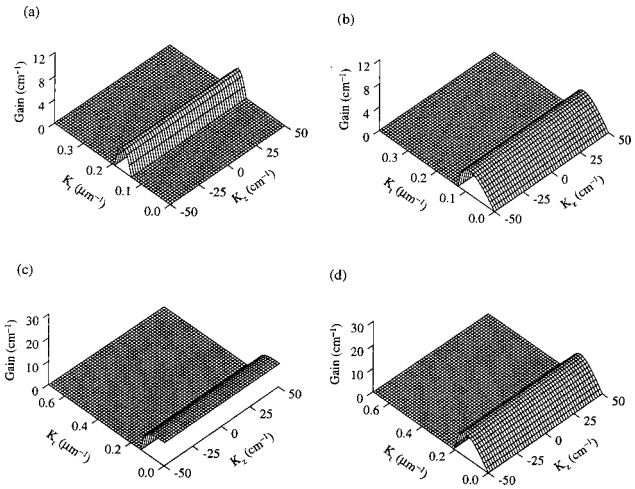

Fig. 8. FFWM-induced gain in **K** space: (a) $P = 8\ \mathrm{cm}^{-1}$, $f = -1$, $\kappa = 10\ \mathrm{cm}^{-1}$; (b) $P = 8\ \mathrm{cm}^{-1}$, $f = -1$, $\kappa = 0$; (c) $P = 20\ \mathrm{cm}^{-1}$, $f = 1$, $\kappa = 10\ \mathrm{cm}^{-1}$; (d) $P = 20\ \mathrm{cm}^{-1}$, $f = 1$, $\kappa = 0$.

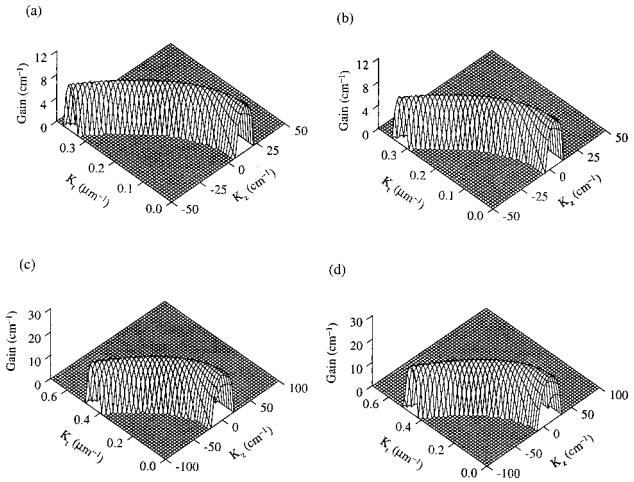

Fig. 9. BFWM-induced gain in **K** space: (a) $P = 8\ \mathrm{cm}^{-1}$, $f = -1$, $\kappa = 10\ \mathrm{cm}^{-1}$; (b) $P = 8\ \mathrm{cm}^{-1}$, $f = -1$, $\kappa = 0$; (c) $P = 20\ \mathrm{cm}^{-1}$, $f = 1$, $\kappa = 10\ \mathrm{cm}^{-1}$; (d) $P = 20\ \mathrm{cm}^{-1}$, $f = 1$, $\kappa = 0$.

Let us consider two examples for $f = \pm 1$. Then Eq. (36) reduces to

$$\omega^2 = -3G^2 + 2G(\kappa - k_\parallel - k_t^2) + (-\kappa + k_\parallel + k_t^2)^2 \qquad f = -1, \tag{37}$$

$$\omega^2 = -3G^2 - 2G(\kappa + k_\parallel + k_t^2) + (\kappa + k_\parallel + k_t^2)^2 \qquad f = 1. \tag{38}$$

Instability gain that is due to BFWM is shown in Figs. 9(a) for $f = -1$ and 9(c) for $f = 1$. Comparing these figures with Figs. 3(b) and 5(b), respectively, one can easily identify BFWM-induced features in Figs. 3(b) and 5(b) at large values of K_t and K_z. At small wave numbers the gain shown in Figs. 3–5 is produced by four-sideband interaction with the forward- and backward-propagating pump waves.

From Eqs. (37) and (38) the largest gain is given by

$$\gamma^{\max} = 2G, \tag{39}$$

with the corresponding wave numbers

$$k_t^2 = G + \kappa - k_\parallel \qquad f = -1, \tag{40}$$

$$k_t^2 = G - \kappa - k_\parallel \qquad f = 1. \tag{41}$$

Figures 9(b) and 9(d) show instability gain for $\kappa = 0$ for two different input powers. Again we conclude that the presence of the grating results in shifting of the BFWM curves but, in this case, along the K_z axis, consistently with Eqs. (40) and (41).

In summary, we have found that some of the features that one can see in Figs. 3–5 originate from two-sideband interaction rather than from interaction among all four sidebands. The grating affects the gain induced by both FFWM and BFWM, shifting them in K_t or in K_z, respectively.

8. EXPERIMENTAL CONSIDERATIONS

Obviously, a linear stability analysis is valid as long as the perturbation amplitude remains small compared with

the cw beam amplitude. When this condition ceases to be satisfied, a numerical analysis should be used. However, we expect the conclusions drawn here to remain qualitatively valid. Our results predict new regions of instability in which self-pulsations occur in both time and space. Such an effect could be observed, for example, in nonlinear waveguides or bulk samples with a grating.

Because grating-induced group-velocity dispersion outside the photonic bandgap depends strongly on the detuning Ω from the edge of the photonic bandgap, we expect the results of our analysis to vary with Ω. Indeed, it was recently demonstrated by Eggleton *et al.*[13] that the period of the pulse train generated through temporal MI in a fiber Bragg grating varies with Ω. In Fig. 10 we plot the periods of spatial modulation, $\Lambda_s = 2\pi/K_t$ (solid curves), and of temporal modulation, $T = 2\pi/(K_z V)$ (dashed curves), that correspond to maximum MI gain in the two cases of [Fig. 10(a)] anomalous and [Fig. 10(b)] normal GVD. Here we plot them as functions of Ω calculated with Eq. (6) rather as than parameter f because Ω can be controlled in laboratory experiment.

Using Fig. 10, we can estimate the size of a sample necessary for experimental observation of MI. Because the typical size of the spatial modulation is $\sim 40\ \mu$m, observing the predicted MI in bulk samples requires a spot size that should exceed roughly 200 μm, resulting in an effective area of $\sim 10^5\ \mu\text{m}^2$. In planar waveguides (two-dimensional geometry), the effective area can be reduced to $\sim 10^3\ \mu\text{m}^2$ but is still relatively large compared with that of optical fiber. As a result, power levels required for observation of spatiotemporal MI are higher than those needed in fiber gratings.

The powers can be significantly reduced by the use of materials with large nonlinear index n_2. One possibility is to use chalcogenide glass, such as As_2S_3 with $n_2 \approx 2 \times 10^{-14}\ \text{cm}^2/\text{W}$ at 1.55 μm,[20,21] which is approximately 100 larger than in silica fibers. Another candidate material is an AlGaAs-integrated Bragg waveguide.[14] When the operating wavelength lies below the half-bandgap of AlGaAs (i.e., near 1.55 μm), the detrimental effects of two-photon absorption can be ignored, and the nonlinear index is $n_2 \approx 1.5 \times 10^{-13}\ \text{cm}^2/\text{W}$. If we estimate incident-beam intensity from the parameters of Fig. 10 we find that $I \approx 9.8\ \text{GW/cm}^2$ for As_2S_3 glass and $I \approx 1.3\ \text{GW/cm}^2$ for an AlGaAs waveguide. Even in these materials, observation of three-dimensional spatiotemporal MI does not appear to be feasible because power levels in excess of 1 MW would be necessary. Note that the increase in optical nonlinearity is often associated with a decrease in the damage threshold. However, in the two-dimensional waveguide geometry with an effective area $\sim 10^3\ \mu\text{m}^2$, required peak powers become ~ 10 kW for the AlGaAs waveguide. The corresponding peak power for As_2S_3 glass is ~ 100 kW. Recently, chalcogenide fibers with an n_2 that is 500 times larger than that in silica fibers were reported.[24] The use of such fibers with larger n_2 will reduce the required peak power to ~ 10 kW. These are typical power levels used in recent experiments with nonlinear propagation effects in fiber Bragg gratings.[25] We should also mention that the longitudinal period of MI is approximately 0.6 cm, which corresponds to a modulation period in time of ~ 50 ps. Thus pulse widths of ~ 1 ns would be large enough for the effects predicted here to be observed.

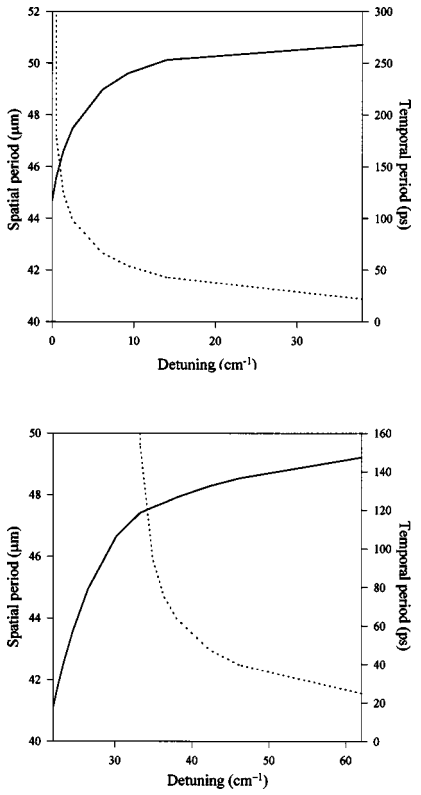

Fig. 10. Spatial period Λ_s (solid curves) and temporal period T (dashed curves) corresponding to maximum MI gain as functions of $|\Omega|$ for (a) anomalous dispersion and (b) normal dispersion with $P = 8\ \text{cm}^{-1}$.

9. CONCLUSIONS

In this paper we have studied spatiotemporal instabilities in periodic bulk Kerr media that occur through an interplay among grating-induced dispersion, diffraction, and nonlinear phase modulation. This problem combines two geometries studied previously: coupled-wave propagation in a one-dimensional periodic structure studied in the context of fiber Bragg gratings[6] and the stability of two counterpropagating waves in a three-dimensional dispersionless Kerr medium considered in the context of plasma physics.[23] As a result, the nonlinear system considered in this study has more degrees of freedom than either of the constituent systems.

It was found that MI in a one-dimensional periodic structure can exist in the normal-dispersion regime (unlike in a uniform medium), though it has a certain threshold below which the system is stable.[6] We have shown that a volume periodic structure may develop instabilities even when the one-dimensional structure is stable. In this case the instability is purely spatial. When the incoming beam intensity reaches a certain threshold level, both spatial and temporal instabilities develop. This result can be visualized as a transverse ring pattern oscillating in time. In general, both spatial and temporal instabilities exist for any incident intensity. At low intensities, the gain curve resembles that for the single-

wave case; i.e., it has a doughnutlike shape with nearly equal gain for frequencies equidistant from the center. At higher intensities, an absolute maximum occurs at $K_z = 0$, which means that the spatial effects again dominate the temporal ones.

An obvious limitation of this and previous analyses[6,8,23] is that the perturbation amplitude is assumed to be small compared with the incident beam's amplitude. When the two amplitudes become comparable, the linear stability analysis is no longer applicable, and a numerical analysis should be used. However, we expect the conclusions drawn here to remain qualitatively valid. We intend to present the results of numerical simulations in future publications.

Whereas our results reduce to known cases in the appropriate limits, we also find parameters for which novel self-pulsations in both time and space occur. Such effects could be observed, for example, in nonlinear planar waveguides or bulk samples with a grating.

ACKNOWLEDGMENTS

The authors thank Taras Lakoba for helpful discussions. This research is supported by the Aileen S. Andrew Foundation, the TRW Foundation, and the National Science Foundation.

Present address, TyCom Laboratories, 250 Industrial Way West, Eatontown, New Jersey 07724; e-mail: nlitchinitser@tycomltd.com.

REFERENCES

1. A. Hasegawa, *Plasma Instabilities and Nonlinear Effects* (Springer-Verlag, Berlin, 1975).
2. G. P. Agrawal, *Nonlinear Fiber Optics*, 2nd ed. (Academic, San Diego, Calif., 1995).
3. C. J. McKinstrie and R. Bingham, "The modulational instability of coupled waves," Phys. Fluids B **1**, 230–237 (1989).
4. C. J. McKinstrie and G. G. Luther, "The modulational instability of collinear waves," Phys. Scr. **T30**, 31–40 (1990).
5. K. Tai, A. Hasegawa, and A. Tomita, "Observation of modulation instability in optical fibers," Phys. Rev. Lett. **56**, 135–138 (1986).
6. C. M. de Sterke, "Theory of modulational instability in fiber Bragg gratings," J. Opt. Soc. Am. B **15**, 2660–2667 (1998).
7. Y. Silberberg, "Collapse of optical pulses," Opt. Lett. **15**, 1282–1284 (1990).
8. L. W. Liou, X. D. Cao, C. J. McKinstrie, and G. P. Agrawal, "Spatiotemporal instabilities in dispersive nonlinear media," Phys. Rev. A **46**, 4202–4208 (1992).
9. G. P. Agrawal, "Modulational instability induced by cross-phase modulation," Phys. Rev. Lett. **59**, 880–883 (1987).
10. C. T. Law and A. E. Kaplan, "Dispersion-related multimode instabilities and self-sustained oscillations in nonlinear counterpropagating waves," Opt. Lett. **14**, 734–736 (1989).
11. B. J. Eggleton, C. M. de Sterke, R. E. Slusher, and J. E. Sipe, "Distributed feedback pulse generator based on nonlinear fiber grating," Electron. Lett. **32**, 2341–2342 (1996).
12. B. J. Eggleton, C. M. de Sterke, and R. E. Slusher, "Nonlinear pulse propagation in Bragg gratings," J. Opt. Soc. Am. B **14**, 2980–2993 (1997).
13. B. J. Eggleton, C. M. de Sterke, A. B. Aceves, J. E. Sipe, T. A. Strasser, and R. E. Slusher, "Modulational instability and multiple soliton generation in apodized fiber gratings," Opt. Commun. **149**, 267–271 (1998).
14. P. Millar, R. M. De La Rue, T. F. Krauss, J. S. Aitchison, N. G. R. Broderick, and D. J. Richardson, "Nonlinear propagation effects in an AlGaAs Bragg grating filter," Opt. Lett. **24**, 685–687 (1999).
15. C. M. de Sterke and J. E. Sipe, "Gap solitons," Prog. Opt. **33**, 203–260 (1994).
16. P. St. J. Russell, "Bloch wave analysis of dispersion and pulse propagation in pure distributed feedback structures," J. Mod. Opt. **38**, 1599–1619 (1991).
17. N. M. Litchinitser, B. J. Eggleton, and D. B. Patterson, "Fiber Bragg gratings for dispersion compensation in transmission: theoretical model and design criteria for nearly ideal pulse compression," J. Lightwave Technol. **15**, 1303–1313 (1997).
18. P. St. J. Russell and J.-L. Archambault, "Field microstructures and temporal and spatial instability of photonic Bloch waves in nonlinear periodic media," J. Phys. (Paris) III **4**, 2471–2491 (1994).
19. Yu. A. Logvin and V. M. Volkov, "Phase sensitivity of a nonlinear Bragg grating response under bidirectional illumination," J. Opt. Soc. Am. B **16**, 774–780 (1999).
20. M. Asobe, "Nonlinear optical properties of chalcogenide glass fibers and their application to all-optical switching," Opt. Fiber Technol. **3**, 142–148 (1997).
21. S. Spälter, G. Lenz, H. Y. Hwang, J. Zimmermann, S.-W. Cheong, T. Katsufuji, R. E. Slusher, "Nonlinear optics in chalcogenide waveguides," presented at the 1999 Annual Meeting of the Optical Society of America.
22. N. M. Litchinitser, B. J. Eggleton, and G. P. Agrawal, "Dispersion of cascaded fiber gratings in WDM lightwave systems," J. Lightwave Technol. **16**, 1523–1529 (1998).
23. G. G. Luther and C. J. McKinstrie, "Transverse modulational instability of collinear waves," J. Opt. Soc. Am. B **7**, 1125–1141 (1990).
24. G. Lenz, J. Zimmermann, T. Katsufuji, M. E. Lines, H. Y. Hwang, S. Spälter, R. E. Slusher, S.-W. Cheong, J. S. Sanghera, and I. D. Aggarwal, "Large Kerr effect in bulk Se-based chalcogenide glasses," Opt. Lett. **25**, 254–256 (2000).
25. B. J. Eggleton, C. M. de Sterke, and R. E. Slusher, "Bragg solitons in the nonlinear Schrödinger limit: experiment and theory," J. Opt. Soc. Am. B **16**, 587–599 (1999).